Evaluation of Euler Solvers for Transonic Wing-Fuselage Geometries

Shreekant Agrawal,* Son François Creasman,† and Robert Byron Lowrie‡
McDonnell Aircraft Company, St. Louis, Missouri 63166

Explicit finite-volume central-difference, implicit finite-volume upwind, and nonconservative upwind solvers are used to compute transonic flowfields of two wing-fuselage geometries. The solutions obtained are evaluated for the overall accuracy and rate of convergence. Results predicted by the three methods are similar, except for some differences in coarse grid regions and near shock locations. The upwind finite-volume scheme is found to yield the best resolution in predicting shock waves, and for any given grid its predictions agree best with the test data. Also, changes in its solution with improved grid resolution are found to be smaller in comparison to those computed by the other two methods. The best level and rate of convergence for these cases are found with the central-difference method, using Runge-Kutta time-stepping and full multigrid schemes.

Introduction

ACCURATE prediction of transonic and supersonic wave drag is critical in fighter aircraft design optimization. The flows are highly nonlinear and require prediction methods that are capable of describing complex phenomena. Although the Euler equations neglect viscous terms, they are capable of describing rotational flows, such as transonic flowfields with shock waves. In addition, a code performance in Euler mode gives valuable insight into the expected performance once viscous terms are included.

There are many numerical methods for approximating solutions to the Euler equations. In general, these methods can be categorized as either central-difference[1-5] or upwind[6-11] schemes. To stabilize the numerical algorithm, both central-difference and upwind schemes contain dissipative terms in their difference form of the governing equations. These terms are necessary to couple neighboring points and to prevent numerical oscillations in regions of severe flowfield gradients, such as near a shock wave or a stagnation point. Two of the major differences between the methods are the manner in which the dissipative terms are implemented and their behavior under various flowfield conditions.

The code chosen to represent the central-difference schemes is FLO67.[4,5] This code integrates the discretized Euler equations using a finite-volume scheme, maintaining conservation of mass, momentum, and energy in each grid cell. Unlike most finite-volume schemes, it stores the flow values at the cell vertices instead of at the cell centers. Convergence to steady-state is accelerated with the use of an explicit five-stage Runge-Kutta scheme, residual smoothing, enthalpy damping, and full multigrid scheme. Like other central-difference schemes, FLO67 adds the dissipation terms explicitly to the governing equations. The magnitude of these dissipative terms can be controlled by the user through two coefficients.

CFL3D[6] was chosen to represent conservative upwind schemes. It incorporates a set of upwind cell-center finite-volume shock-capturing algorithms that use either Roe's flux-difference splitting[7] or Van Leer's flux-vector splitting technique.[8] For this study, CFL3D was run using the flux-difference splitting scheme of Roe, as this scheme is considered to have less natural dissipation and, hence, more sharply defined shocks. Roe's scheme contains dissipative terms derived through one-dimensional characteristic theory, and, therefore, generally models wave propagation better than central-difference methods. To further control numerical oscillations near shock waves, CFL3D incorporates a flux-limiting scheme.[9] Since the algorithm is an implicit time-stepping method, solutions can be obtained at large CFL numbers. As with FLO67, convergence to steady state can be achieved through the multigrid option. When compared to central-difference methods, the number of algebraic operations in upwind schemes (and, therefore, the cost per iteration) is generally higher.

Recently, a nonconservative finite-difference upwind formulation of the Euler equations has shown promise for supersonic flows.[10] The isentropic form of this formulation has also been incorporated in the ET2 code[11] for predicting transonic flowfields. The method differs from other upwind methods in that the Euler equations are expressed in terms of Riemann variables in a streamline coordinate system, which allows upwind differencing in a true sense. The formulation, therefore, accurately models wave propagation. However, its lack of conservation, along with the isentropic assumption, is especially apparent across shock waves. The isentropic assumption has been somewhat circumvented for supersonic flows by incorporting a shock-fitting scheme for the outer bow shock,[10] but a general three-dimensional shock-fitting procedure has yet to be implemented in the ET2 code.

Even though these formulations of Euler equations have been successfully applied in different applications in two and three dimensions, more comparisons between methods are needed. The accuracy and efficiency of the various methods should be examined for complex three-dimensional problems. The intent of this paper is to begin addressing these issues by presenting the differences in transonic solutions obtained from the three solvers on simple wing-fuselage geometries. Comparisons are presented for the RAE[12] and the F-15[13] wing-fuselage configurations in transonic flowfields.

Grid Topology

The grid topology used is a C-O type, which is C-like in the chordwise direction and O-like around the fuselage. The grids were generated by the PGRID code.[14] PGRID generates a three-dimensional body-conforming grid about arbitrary wing-fuselage configurations. The code is based on a conformal mapping technique, with elliptic smoothing for the field

Received Aug. 2, 1990; presented as Paper 90-3015 at the AIAA 8th Applied Aerodynamics Conference, Portland, OR, Aug. 20-22, 1990; revision received Nov. 9, 1990; accepted for publication Nov. 9, 1990.

*Technical Specialist, Aerodynamics, CFD Project. Associate Fellow AIAA.
†Engineer, Aerodynamics, CFD Project. Member AIAA.
‡Engineer, Aerodynamics, CFD Project; currently at the University of Michigan, Ann Arbor, MI. Member AIAA.

points. This topology was selected for its ability to better resolve the fuselage flowfields. Given a number of total grid points, this topology places approximately three times the number of grid points on the fuselage when compared to a C-H topology.

Computational grids generated by the PGRID code for the RAE[12] and F-15[13] wing-fuselage geometries are shown in Fig. 1. Only the surface and symmetry grid planes are shown. For both configurations, the aft end of the fuselage includes a sting that extends to the downstream farfield. The RAE wing-fuselage is a generic geometry with a wealth of experimental data. The F-15 geometry is representative of present fighter aircraft. Note that the PGRID analytical representation of the fuselage shape requires the F-15 fuselage to be smoothed to eliminate any discontinuities on the surface (i.e., faired inlet). As a result, the grid shown only approximates the actual F-15 fuselage geometry. The overall grid dimensions are 161 (streamwise), 25 (normal), and 33 (spanwise), resulting in a total of 97 chordwise (upper and lower) and 25 spanwise points on the wing surface, and 161 × 25 points on the fuselage surface, including the sting. Computational grids of dimensions 225 (streamwise), 33 (normal), and 33 (spanwise) were also used (not shown here) in a grid sensitivity analysis. This resulted in a total of 177 × 25 points on the wing, and 225 × 33 points on the fuselage.

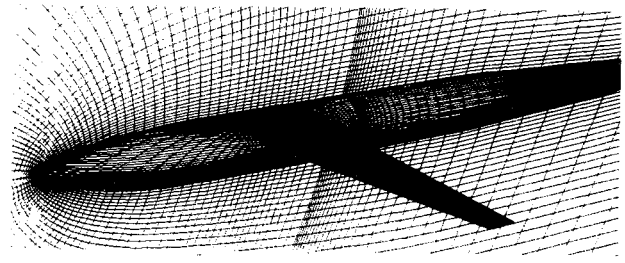

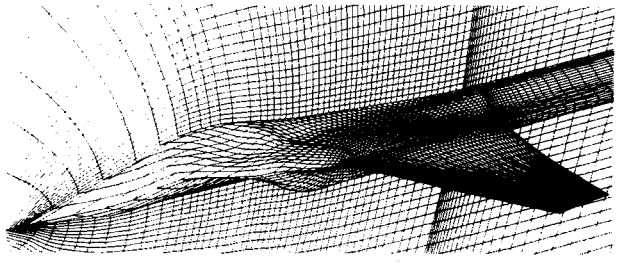

Fig. 1 Wing-fuselage grid on the surface and symmetry plane; grid size: 161×25×33 (half-plane).

Results

To accurately predict wing-fuselage flowfields, the flow solvers (FLO67, CFL3D, and ET2) were modified for the PGRID topology. The flowfield predictions for both the RAE and F-15 are presented in Figs. 2–11. For the RAE wing-fuselage configuration, results were obtained at $M_\infty = 0.9$ and $\alpha = 1.0$ deg. Computed and experimental wing pressure distributions at two span stations are shown in Fig. 2. The grid size for this case is 161×25×33 (132,825 points). At 25% semispan location, the three methods compare well with experiment (Fig. 2). However, at the outboard stations on the wing, there are significant differences in the solutions, particu-

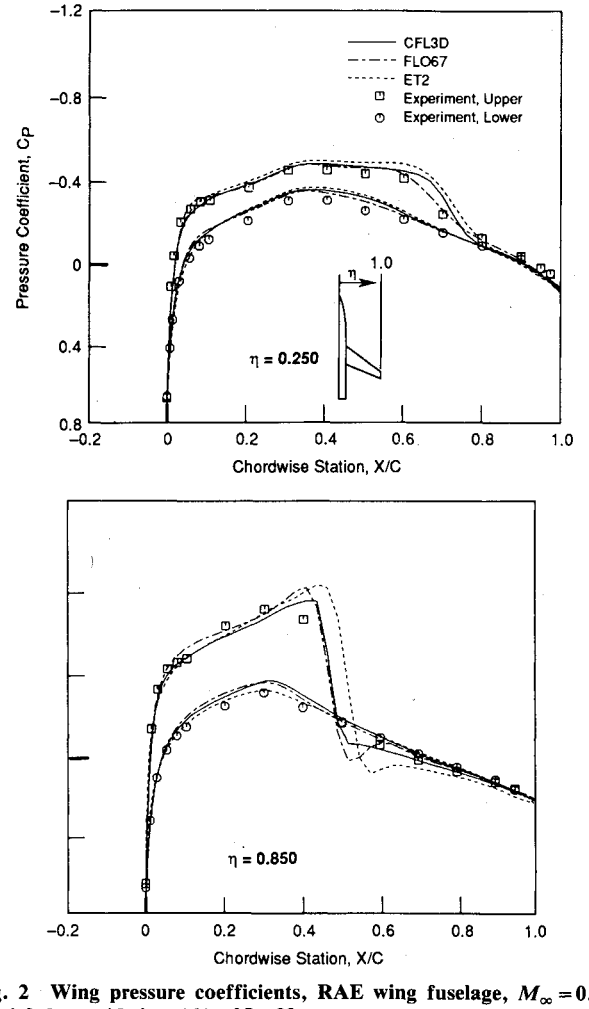

Fig. 2 Wing pressure coefficients, RAE wing fuselage, $M_\infty = 0.9$, $\alpha = 1.0$ deg; grid size: 161×25×33.

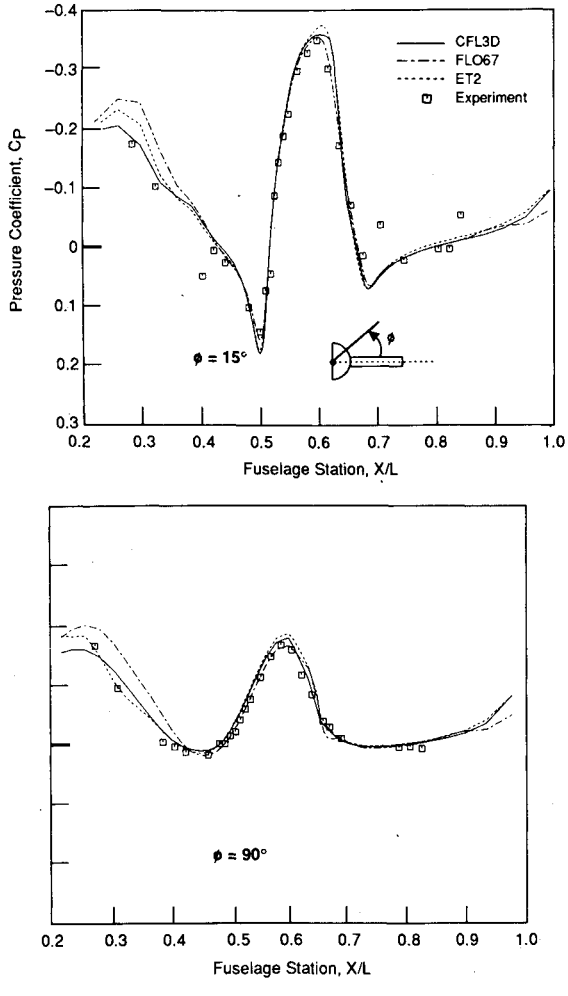

Fig. 3 Fuselage pressure coefficients, RAE wing fuselage, $M_\infty = 0.9$, $\alpha = 1,0$ deg; grid size: 161×25×33.

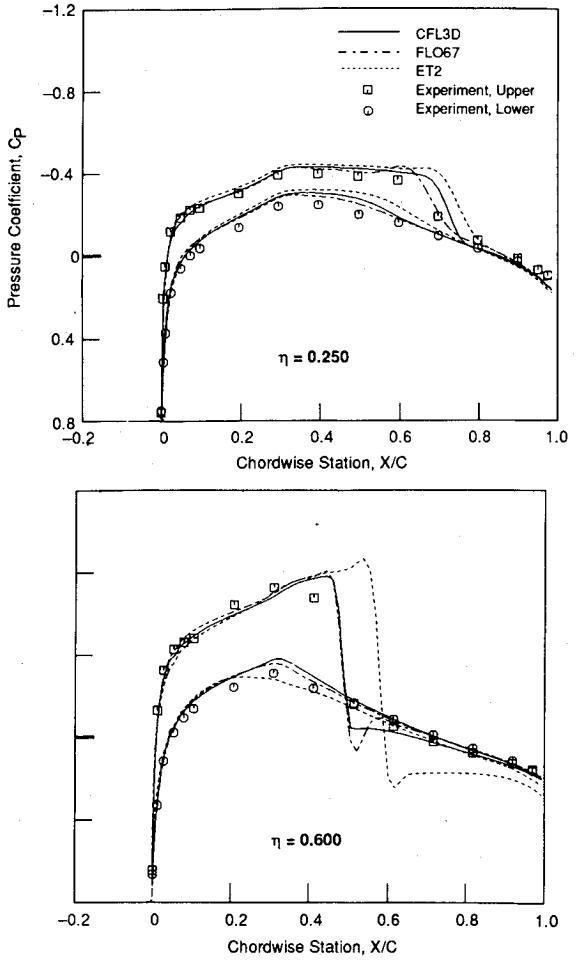

Fig. 4 Wing pressure coefficients, RAE wing fuselage, $M_\infty = 0.9$, $\alpha = 1.0$ deg; grid size $225 \times 33 \times 33$.

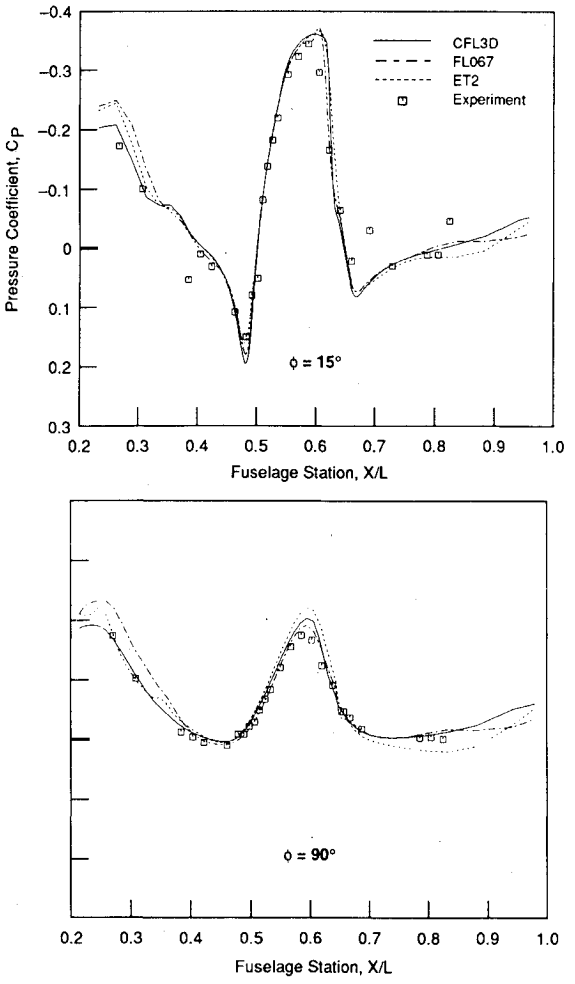

Fig. 5 Fuselage pressure coefficients, RAE wing fuselage, $M_\infty = 0.9$, $\alpha = 1.0$ deg; grid size: $225 \times 33 \times 33$.

larly in the predicted shock locations. The two conservative methods predict nearly identical shock locations. It is interesting to note that the nonconservative method (ET2) predicts the shock location approximately 5% chord downstream of the experimental data and to those predicted by the conservative methods. Near the leading edges, predictions compare quite well and are nearly identical.

FLO67 shows pre- and postshock oscillations typical of its numerical scheme. This problem can be minimized by manipulating the dissipative coefficients. The oscillations are also observed in the ET2 solutions. CFL3D shows the best shock definition, as a result of Roe's upwind scheme and the total-variation diminishing (TVD) scheme, both of which are implemented in the code.

The RAE fuselage pressure distributions from the three methods are shown in Fig. 3, where pressure coefficient is plotted against fuselage station for longitudinal cuts at two angular locations (ϕ). The pressure distributions compare quite well with experimental data, except near the nose and aft end of the fuselage. This is perhaps due to the inadequate grid resolution in this region. The upwind codes appear to do a better job of resolving the nose region, with CFL3D predicting the most accurate solution. At $\phi = 90$ deg, ET2 predictions near the nose compare surprisingly well with experiment. In the aft end regions of the fuselage, all three codes perform very similarly. The reasons for poor agreement at certain points near the aft end are not clear.

In an effort to improve the results, the codes were run on a finer grid of size $225 \times 33 \times 33$ (245,025 points). Wing and fuselage pressure comparisons corresponding to this grid size are shown in Figs. 4 and 5, respectively. For clarity purposes, grid refinement results from the different codes are also shown in Fig. 6, at the same spanwise location (60%) on the wing and the same angular location ($\phi = 60$ deg) on the fuselage. For the wing comparisons, note the changes in solution predicted by ET2 on the lower surface and near the shock wave (Fig. 6), where the solution change is found to be the largest.

In general, predicted shocks are more pronounced with this grid density than with the coarser grid. Although the shock locations computed by CFL3D and FLO67 are nearly identical, ET2 predictions worsen with grid refinement (Fig. 6). ET2 now predicts the shocks approximately 10% chord downstream of the experimental data, as opposed to only 5% for the coarser grid (see Figs. 2 and 4). This trend is consistent for all spanwise stations. The shock oscillations predicted by FLO67 and ET2 appear slightly worse, presumably a result of the reduced dissipation level. The FLO67 dissipation coefficients were kept constant for both grid sizes. Lower surface pressure peaks predicted by the three methods are found to be quite different. Although grid refinement was expected to minimize these differences, Figs. 2 and 4 do not indicate so. The reasons for such differences are not yet clear.

As far as solutions on the fuselage are concerned (Figs. 5 and 6), the predictions at the suction peak in the proximity of the wing ($X/L \sim 60\%$) are slightly worsened. Although there is solution improvement, due to the increased grid resolution near the fuselage nose regions, it is only marginal. Solutions near the fuselage aft end are found to change significantly for ET2. Increasing the grid resolution further with this topology appears to be of little benefit.

It is interesting to note that CFL3D overall predicts the least change in solution on both the wing and the fuselage, due to grid refinement. We do not claim that these solutions are grid converged, but it does appear that, for a given grid size, CFL3D predicts solutions more accurately than FLO67 and ET2.

The upper surface (top view) pressure contours computed with the three methods for the RAE geometry are shown in Fig. 7 for both grid sizes. Overall, the contours appear similar except for some minor differences near the nose and aft ends of the fuselage. Pre- and postshock pressure oscillations in the FLO67 and ET2 solutions are also evident on the wing surface. The poor grid resolution near the fuselage nose is apparent from the jagged contours in this region. A different grid topology (H-O type) on the fuselage is expected to improve solutions near the nose regions.

For the F-15 wing-fuselage configuration, results were obtained at $M_\infty = 0.9$ and $\alpha = 4.84$ deg. The wing surface pressure distributions are shown in Fig. 8 for two span stations. Results are presented for a grid size of $161 \times 25 \times 33$. In spite of the fuselage geometry approximation and the inlet fairing, computed results compare reasonably well with experiment. For this case, the nonconservative ET2 code predicts the leading-edge suction peak very well at the inboard station (36.2%), whereas at the outboard station its results are noticeably worse in comparison to the two conservative codes. Results computed with CFL3D and FLO67 are very similar at most span stations. The prediction of shock location with ET2 does not compare well with experiment, even though it is only a few percent chord downstream of that computed by CFL3D and FLO67. This observation is also consistent with the ET2 results for the RAE configuration. Both FLO67 and CFL3D

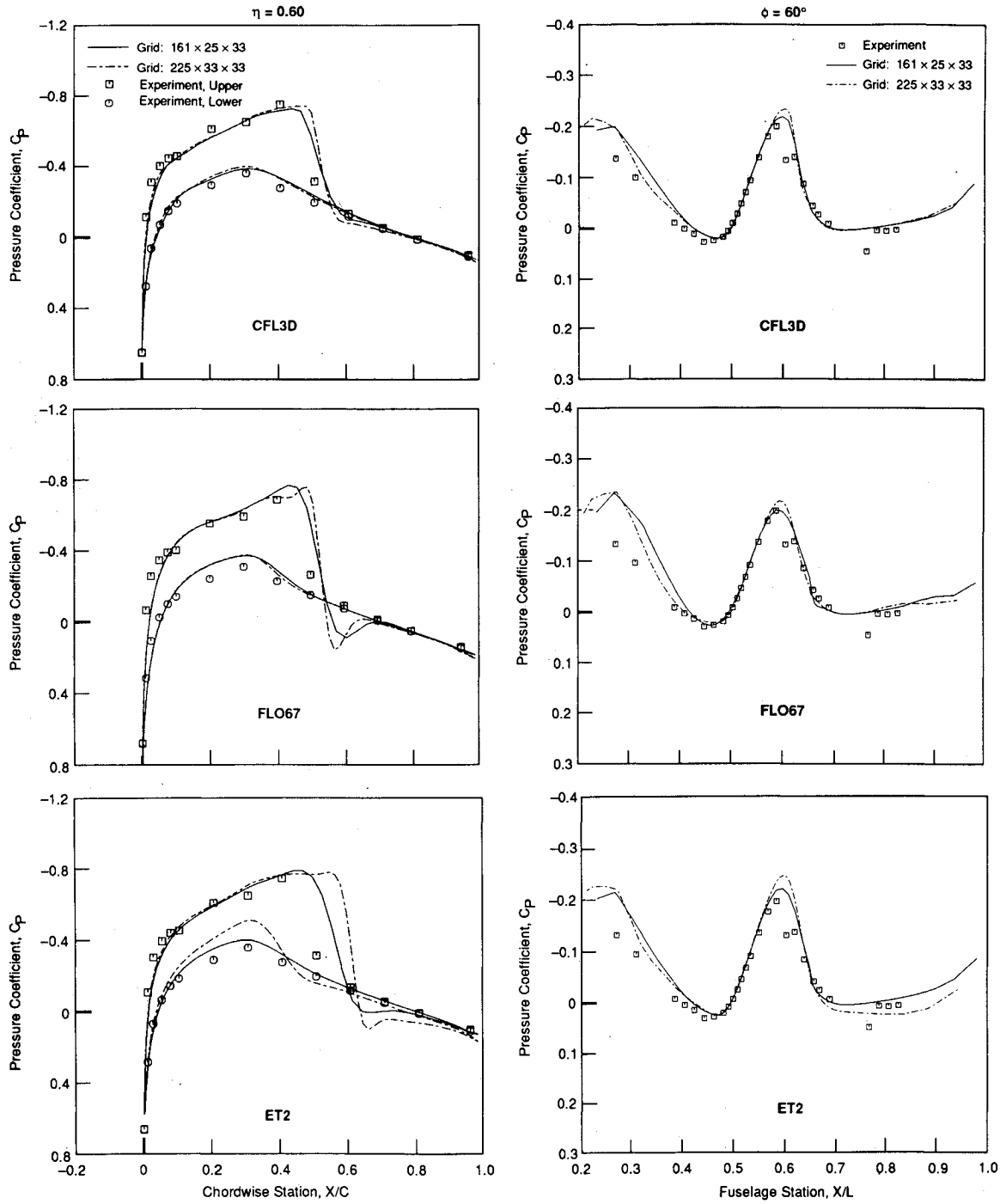

Fig. 6 Effect of grid refinement on RAE wing and fuselage solutions, $M_\infty = 0.90$, $\alpha = 1.0$ deg.

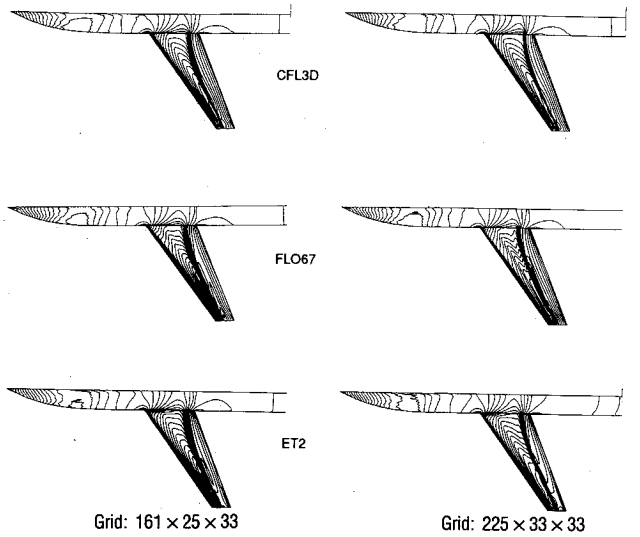

Fig. 7 Pressure contours, top view of RAE wing fuselage, $M_\infty = 0.90$, $\alpha = 1.0$ deg.

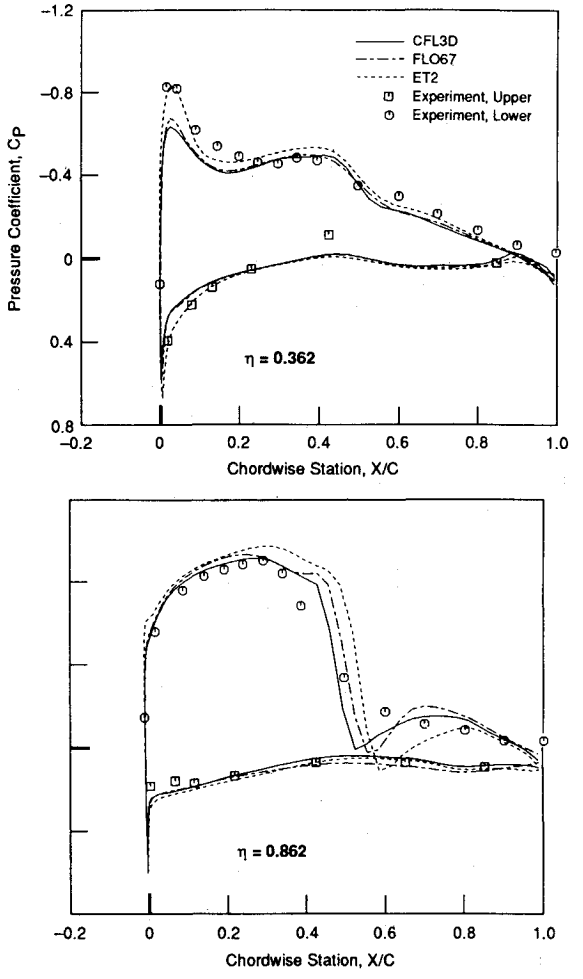

Fig. 8 Wing pressure coefficients, F-15 wing fuselage, $M_\infty = 0.9$, $\alpha = 4.84$ deg; grid size: $161 \times 25 \times 33$.

predict very similar shock locations, except at the most outboard station (86.2%), where the shock predicted by FLO67 is slightly downstream of that predicted by CFL3D. Once again, CFL3D computed shocks appear crisper than those computed by FLO67 and ET2. In general, the magnitudes of pressure overshoot computed by FLO67 and ET2 solutions for the F-15 are smaller than those in the RAE configuration. The trailing-edge pressures are overpredicted by all of the codes, indicating

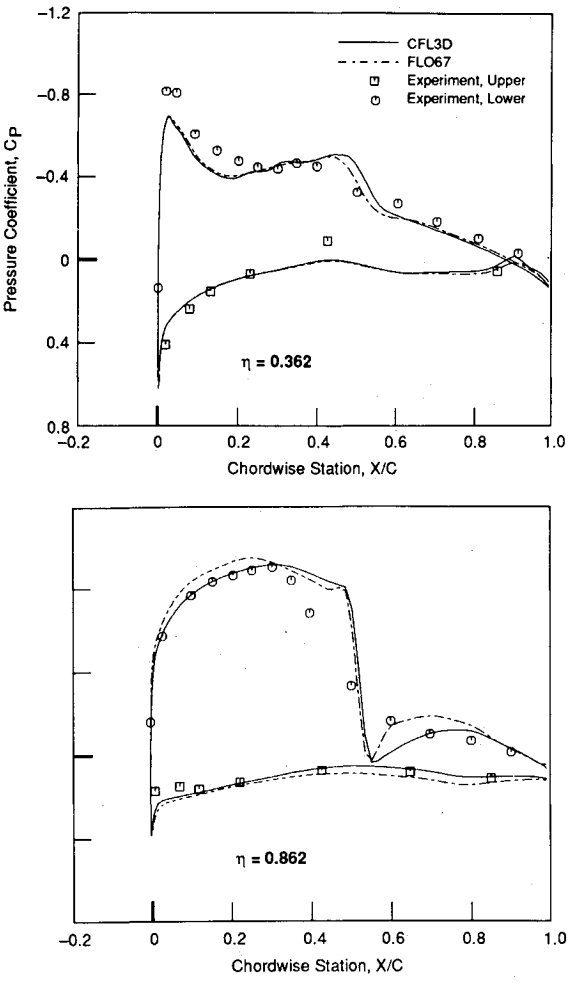

Fig. 9 Wing pressure coefficients, F-15 wing fuselage, $M_\infty = 0.9$, $\alpha = 4.84$ deg; grid size: $225 \times 33 \times 33$.

that perhaps the flow is separated in this region and that viscosity may be a factor here.

As with the RAE configuration, solutions for the F-15 were also obtained on a finer grid of size $225 \times 33 \times 33$. Wing pressure comparisons corresponding to this grid size are shown in Fig. 9. Only CFL3D and FLO67 results are shown. ET2 encountered some convergence problems with the increased grid dimensions. For clarity purposes again, grid refinement results from CFL3D and FLO67 are shown in Fig. 10 at the same wing spanwise location (58.7%). Changes in solution near the leading edges are minor, although a slight improvement is observed (Figs. 8 and 9) for both codes. Predicted shocks are more pronounced with this grid density than those with the coarser grid. Although the shock location predicted by CFL3D is slightly downstream of that predicted by FLO67, the shock strengths computed by both codes are very similar. This trend is consistent for all spanwise locations.

For all the solutions shown above, the average residuals were reduced by at least three orders of magnitude. In addition, all the cases were run to a point where the changes in force and moment coefficients were virtually negligible (less than 0.1%). At that point, the solutions were assumed to be converged. Figure 11 shows a few typical plots for the average residual and lift coefficient histories for each of the three codes. All solutions were executed on a Convex C-1 computer. The CPU run time and the residual values corresponding to the points where the solutions were assumed converged are shown in Table 1. Note the performance of FLO67, where the level and rate of convergence are markedly better than those of the other two codes. Rate of convergence for CFL3D is also considered to be very compatible. This is in part a result of the

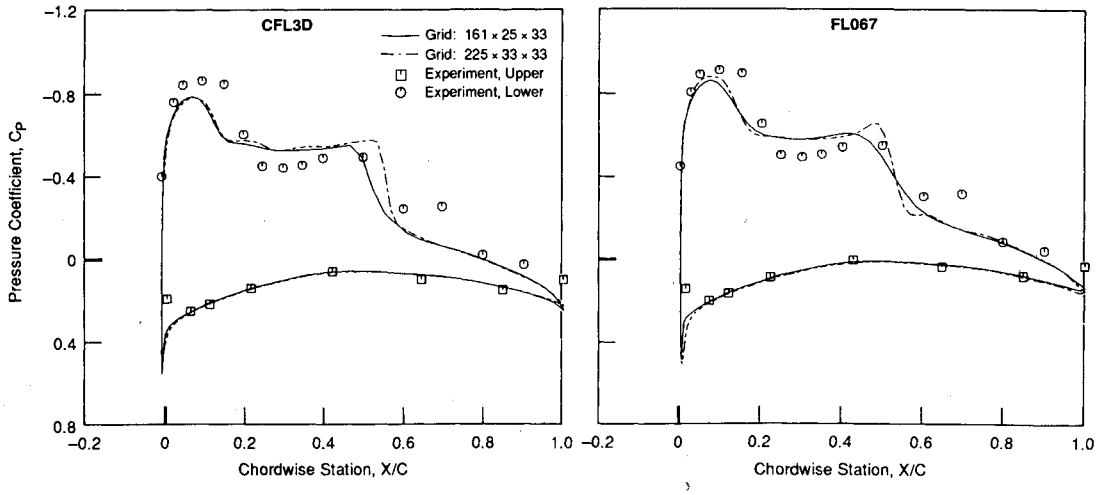

Fig. 10 Effect of grid refinement on F-15 wing-fuselage solutions, $M_\infty = 0.9$, $\alpha = 4.84$ deg, $\eta = 0.587$.

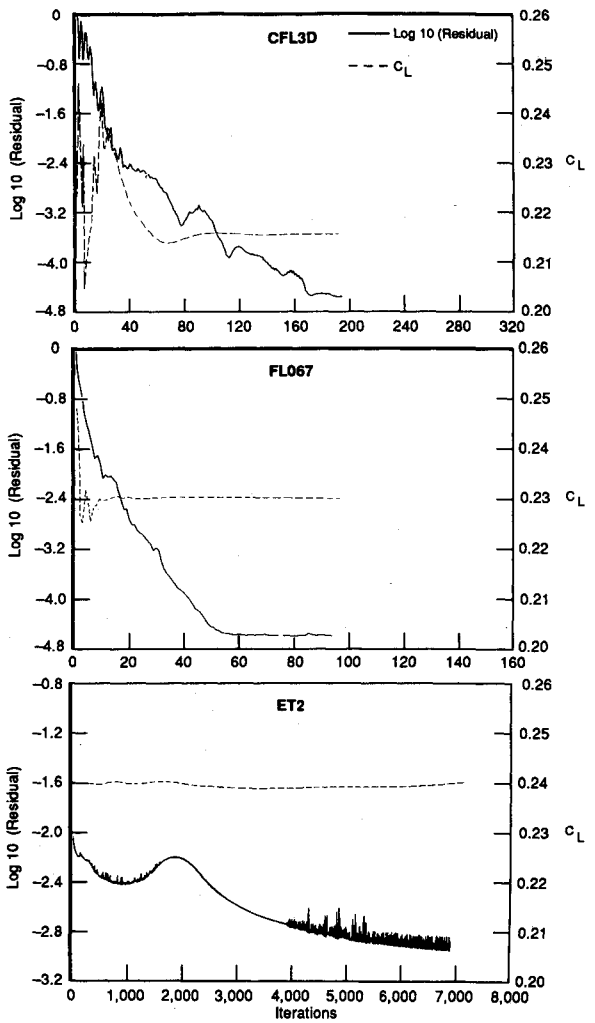

Fig. 11 Residual and lift histories, F-15 wing-fuselage configuration, $M_\infty = 0.90$, $\alpha = 4.84$ deg; grid: $161 \times 25 \times 33$.

multigrid convergence acceleration scheme implemented in FLO67 and CFL3D. The CPU time for CFL3D is, in general, two to three times longer than for FLO67. It should be mentioned here that both grid sequencing and multigrid schemes were used for FLO67 solutions, whereas for CFL3D solutions only multigrid was used. ET2 uses a more primitive point-Jacobi scheme with "checkerboarding," which helps explain its very slow convergence rate.

Table 1 Comparison of convergence and CPU run time[a]

Flow solver	Config.	Grid size[b]	No. of iterations	Log_{10} (Aver. Res.)	Convex C-1 CPU time, h
CFL3D	F-15	Coarse	150	−3.8	2.4
		Fine	200	−3.0	6.5
	RAE	Coarse	200	−4.3	4.3
		Fine	300	−3.5	14.0
FLO67	F-15	Coarse	70	−4.4	1.3
		Fine	100	−3.0	4.0
	RAE	Coarse	80	−5.0	1.4
		Fine	90	−3.5	4.7
ET2	F-15	Coarse	7080	−3.0	49.0
		Fine	—	—	—
	RAE	Coarse	6300	−4.0	55.4
		Fine	4860	−3.5	81.6

[a]Multigrid and grid sequencing options were used for FLO67, only multigrid for CFL3D, only grid sequencing for ET2. Invariant force coefficients were used as convergence guideline for all solutions.
[b]Definitions: coarse = $161 \times 25 \times 33$ points, fine = $225 \times 33 \times 33$ points.

Finally, the force and moment coefficients obtained with the three codes are summarized in Table 2, for both configurations. The integrated coefficients are also shown for the geometry pertaining to the wing only. In the calculation of integrated coefficients, the contribution of sting is not included. Since the experimental force and moment coefficients are not available, the median values of the respective coefficients are used as the reference in this discussion. The differences in the results from the three solvers are clearly reflected in this table. A comparison of the coefficients reveals a deviation range (from the median) of as much as ±31% for the drag coefficients. When the contribution of the fuselage is included, this deviation range increases to 54%. A deviation range of 20% is found for the lift coefficients when comparing both wing and wing-fuselage results. Looking at the moment coefficients, a 30% deviation range is found for the wing and 40% for the wing-fuselage results.

Accepting the median values as the reference, CFL3D consistently underpredicts the lift coefficients. FLO67-calculated lift coefficients fall close to the median values, whereas ET2 tends to overpredict this force parameter. However, FLO67-computed drag coefficients are markedly higher than those predicted by the other two codes, ranging 20–31% from the wing and wing-fuselage median values. The discrepancy may be a result of the significant differences in the predicted lower surface pressure peaks. The observed trend of the moment

Table 2 Summary of force and pitching moment coefficients predicted by the three codes

Flow solver	Config.	Grid size[a]	Wing			Wing/Fuselage		
			C_L	C_D	C_M	C_L	C_D	C_M
CFL3D	F-15	Coarse	0.1365	0.0042	−0.0473	0.2141	0.0166	−0.0194
		Fine	0.1419	0.0049	−0.0439	0.2145	0.0155	−0.0132
	RAE	Coarse	0.1054	0.0062	−0.0706	0.1293	0.0136	−0.0572
		Fine	0.1071	0.0053	−0.0717	0.1316	0.0104	−0.0601
FLO67	F-15	Coarse	0.1473	0.0050	−0.0542	0.2306	0.0199	−0.0263
		Fine	0.1503	0.0051	−0.0495	0.2266	0.0184	−0.0176
	RAE	Coarse	0.1152	0.0078	−0.0807	0.1396	0.0201	−0.0684
		Fine	0.1162	0.0072	−0.0816	0.1408	0.0177	−0.0710
ET2	F-15	Coarse	0.1559	0.0042	−0.0536	0.2406	0.0175	−0.0274
		Fine	—	—	—	—	—	—
	RAE	Coarse	0.1240	0.0066	−0.0856	0.1502	0.0123	−0.0754
		Fine	0.1313	0.0055	−0.0963	0.1597	0.0126	−0.0982

[a]Definitions: coarse = $161 \times 25 \times 33$ points, fine = $225 \times 33 \times 33$ points.

coefficients predicted by the codes is similar to that of the lift coefficients.

The table shows that the grid refinement does have a significant effect on the obtained solutions. A change of as much as 33% is found for the FLO67 computed wing-fuselage moment coefficients, and as little as 0.2% going from coarse to fine grid for the CFL3D computed wing-fuselage lift coefficients (F-15 solutions). For all of the solutions, the wing-fuselage lift coefficients are consistently predicted by the conservative codes (FLO67 and CFL3D). This is supported by the small solution changes (0.2–2.0%), due to the grid refinement. A change of 6.3% is found for the lift coefficients (RAE solutions) computed by the nonconservative code (ET2). The wing-fuselage drag coefficients are not as consistently predicted by any of the codes. CFL3D solutions have a change of 6% for the F-15 configuration and a change of 23% for the RAE configuration. For FLO67, the change is 8% for the F-15 and 12% for the RAE. ET2 shows a small change of 2% for its RAE solutions. The wing-fuselage moment coefficients are also inconsistently predicted by the codes. For CFL3D, changes of 32% and 5% are found in its F-15 and RAE solutions, respectively. FLO67 solutions have changes of 33% for the F-15 and 4% for the RAE. A 30% change is found for the ET2 solutions on the RAE configuration.

Conclusions

Three different Euler solvers using different formulations are evaluated for their overall solution accuracy and efficiency in predicting transonic flowfields on wing-fuselage configurations. These solvers are based on a conservative central-difference method (FLO67), a conservative upwind method (CFL3D), and a nonconservative upwind method (ET2). Two geometries, the RAE and the F-15, have been analyzed. Results predicted by the three methods are generally found to be similar, except for some differences near the fuselage nose, wing leading edges, and near shock locations. As expected, the upwind conservative code (CFL3D) predicts shock waves in the most consistent and accurate manner. For a given grid, its predictions agree best with the test data, and changes in its solution with improved grid resolution are found to be smaller than those obtained with FLO67 and ET2. ET2 does a surprisingly good job, considering that it is based on a nonconservative formulation with no shock-fitting scheme implemented. The best level and rate of convergence are found with the central-difference method (FLO67), using Runge-Kutta time-stepping and full multigrid schemes. This code is particularly robust, and its results may suffice for most engineering applications.

Acknowledgments

This study was supported by the McDonnell Douglas Independent Research and Development program. The authors would like to express their sincere thanks to James L. Thomas of NASA Langley Research Center for providing assistance and fruitful discussions.

References

[1]Jameson, A., Schmidt, W., and Turkel, E., "Numerical Solutions of the Euler Equations by Finite Volume Methods Using Runge-Kutta Time-Stepping Schemes," AIAA Paper 81-1259, June 1981.

[2]Jameson, A., and Baker, T. J., "Solution of the Euler Equations for Complex Configurations," AIAA Paper 83-1929, July 1983.

[3]Agarwal, R. K., and Deese, J. E., "Transonic Wing-Body Calculations Using Euler Equations," AIAA Paper 83-0501, Jan. 1983.

[4]Jameson, A., "A Vertex Based Multigrid Algorithm for Three-Dimensional Compressible Flow Calculations," *Numerical Methods for Compressible Flows—Finite Difference, Element, and Volume Techniques,* ASME-AMD-Vol. 78, Dec. 1986, pp. 45–73.

[5]Volpe, G., Siclari, M. J., and Jameson, A., "A New Multigrid Euler Method for Fighter-Type Configurations," AIAA Paper 87-1160, June 1987.

[6]Thomas, J. L., Taylor, S. L., and Anderson, W. K., "Navier-Stokes Computations of Vortical Flows over Low Aspect Ratio Wings," AIAA Paper 87-0207, Jan. 1987.

[7]Roe, P. L., "Approximate Riemann Solvers, Parameter Vectors, and Difference Schemes," *Journal of Computational Physics,* Vol. 43, No. 2, 1981, pp. 357–372.

[8]Van Leer, B., "Flux-Vector Splitting for the Euler Equations," ICASE Rept. 82-30, Sept. 1982.

[9]Chakravarthy, S. R., "The Versatility and Reliability of Euler Solvers Based on High-Accuracy TVD Formulations," AIAA Paper 86-0243, Jan. 1986.

[10]Verhoff, A., Stookesberry, D. C., Hopping, B. M., and Michal, T. R., "Supersonic-Hypersonic Flowfield Prediction Method for Aircraft Configurations," *Fourth Symposium on the Numerical & Physical Aspects of Aerodynamic Flows,* Jan. 1989.

[11]Agrawal, S., Vermeland, R. E., Verhoff, A., and Lowrie, R. B., "Euler Transonic Solutions over Finite Wings," AIAA Paper 88-0009, Jan. 1988.

[12]Treasgold, D. A., Jones, A. F., and Wilson, K. H., "Pressure Distribution Measured in the RAE 8 ft × 6 ft Transonic Wind Tunnel on RAE Wing 'A' in Combination with an Axi-Symmetric Body at Mach Numbers of 0.4, 0.8, and 0.9," AGARD-AR-138, May 1979, Chap. B-4.

[13]Anderson, R. M., "Wind Tunnel Test on the 4.7 Percent Scale F-15 in the McDonnell Douglas Polysonic Wind Tunnel," Rept. MDC A0974, Vol. I-III, Aug. 1971.

[14]Chen, L. T., Vassberg, J. C., Chang, K. C., and Cebeci, T., "A Transonic Wing/Body Flowfield Computational Method using a General Grid Generation Scheme and an Inverse Boundary-Layer Method," Rept. MDC J3773-1, Vol. I, Jan. 1986.